Journal of
Materials Chemistry A

Accepted Manuscript

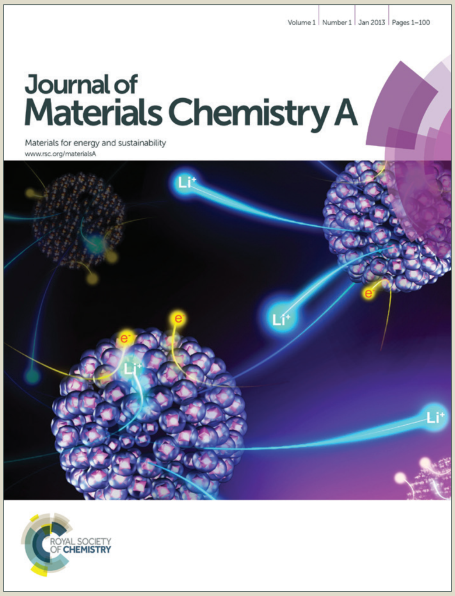

ROYAL SOCIETY
OF CHEMISTRY

www.rsc.org/materialsA

Journal of Materials Chemistry A RSCPublishing

ARTICLE

Cite this: DOI: 10.1039/x0xx00000x

Received 00th January 2012,
Accepted 00th January 2012

DOI: 10.1039/x0xx00000x

www.rsc.org/

Soft Templated Mesoporous Manganese Oxide/Carbon Nanotube Composite via Interfacial Surfactant Assembly

Chang-Wook Lee,[a] Seung-Beom Yoon,[a] Seong-Min Bak,[a] Joah Han,[b] Kwang Chul Roh*[b] and Kwang-Bum Kim*[a]

A mesoporous manganese oxide/carbon nanotube (CNT) composite was successfully synthesized using cetyltrimethylammonium bromide as a protection layer to prevent the direct contact between CNT and MnO_4^- ions, a linking agent to interact with MnO_4^- ions and a structure-directing agent for the formation of mesoporous oxide. The observed improvement in electrochemical utilization of MnO_2 was due to the synergetic effect of the mesoporous structure and CNTs, which enhanced the overall electronic and ionic conductivities.

Introduction

Mesoporous materials are a relatively new class of material, characterized by a high specific surface area (~1,000 $m^2\ g^{-1}$) and the presence of mesopores with diameters in the range of 2–10 nm. They are actively used in applications that require easily accessible uniform mesopores.[1-3] Since the discovery of M41S silica molecular sieves in 1992, considerable effort has been devoted to extending the mesoporous family to include transition metal oxides. Such materials have many potential applications ranging from catalysts, absorbents, and gas sensors, to energy storage devices such as batteries and electrochemical capacitors.[4-6] In spite of those excellent properties, the poor electrical conductivity restricts the application of mesoporous materials. Therefore, the development of a novel synthetic route to prepare mesoporous oxides with enhanced electrical conductivity is crucial. In order to achieve this aim, the combination of mesoporous oxides with carbonaceous materials, such as carbon nanotubes (CNTs), carbon nanofibers (CNFs), or graphene, is a potential route. In particular, CNTs, with their 3D nanoporous structure and 1D electron conduction path, are considered to provide an ideal composite template owing to their chemical stability, good electrical conductivity, and large surface area.[7, 8] Therefore, a mesoporous oxide/CNT composite could be an attractive material for a wide variety of applications, owing to its high surface area, large pore size, and good electrical conductivity. A number of studies regarding the synthesis of such materials have recently been reported;[9-12] however, these have highlighted the difficulties associated with the preparation of non-siliceous mesoporous materials, which arise from the increased complexity in controlling hydrolysis–condensation processes on the CNT surface. A small number of papers regarding non-siliceous oxide/CNT composites have been published.[12, 13] Bak *et al*. reported the synthesis of a uniformly coated mesoporous $Ni(OH)_2$/CNT composite using a complex process of electroless deposition in the presence of a highly concentrated lyotropic liquid-crystal hard template (Brij 56).[12]

In this study, we proposed the novel synthesis to prepare meso-MnO_2/CNT via interfacial surfactant assembly. So far, numerous papers have been published on the synthesis of MnO_2/carbon nanocomposites using redox deposition since it is simple and straightforward (i.e. immersion of CNTs into $KMnO_4$ solution).[14-18] The proposed reaction mechanism for this approach is as follows:

$$4MnO_4^- + 3C + H_2O \rightarrow 4MnO_2 + CO_3^{2-} + 2HCO_3^-$$

While the redox deposition is very useful for simple and scalable synthesis of MnO_2/CNT composite, CNTs react with MnO_4^- ions directly and is gradually consumed at the expense of MnO_2 deposition.[16-18] The carbon oxidation leads to carbon consumption and collapse of carbon bonding structures that degrade the electrical conductivity of carbon. Therefore, it is practically important to investigate the synthesis of MnO_2/CNT composite which does not damage carbon during the composite synthesis. To protect CNT from redox reaction with MnO_4^- ions, we proposed two approaches; (i) blocking the direct contact between CNT and MnO_4^- ions and (ii) using ethanol as a reducing agent of MnO_4^- ions. For that, firstly CNT was coated with the cationic surfactant cetyltrimethylammonium bromide (CTAB). Then, the surfactant dissociates to CTA^+ coated on CNT and Br^- ions in aqueous solution, and the positively charged CTA^+ and negatively charged MnO_4^- ions self-assemble on CNT. Secondly, we used ethanol as a reducing agent to reduce MnO_4^- ions to MnO_2. Alcohol oxidation by $KMnO_4$ is well known[19], however, little studies are available on the synthesis of MnO_2/CNT composites. To the best of our knowledge, this is the first report on the synthesis of meso-MnO_2/carbon nanocomposite using ethanol reduction.

In the present study, mesoporous MnO_2/CNT composites were successfully synthesized using the simple and reliable concept of interfacial surfactant assembly on the CNT surface. The cationic surfactant CTAB acts as a protection layer to prevent the direct contact between CNT and MnO_4^- ions, a linking agent to interact with MnO_4^- ions and a structure-directing agent for the formation of mesoporous oxide. To verify the utility of the MnO_2 composite for pseudocapacitor applications, we evaluated its electrochemical properties.

Experimental

Preparation

For synthesis of the mesoporous MnO_2/CNT composite, 169 mg of bare CNTs (multiwalled CNTs, ILJIN Nanotech) were dispersed in 135 mL of distilled H_2O with 1.69 g of CTAB. Next, 15 mL of a 0.1 M $KMnO_4$ (>99%, Aldrich) aqueous solution was added to the CTA^+/CNT suspension and stirred for 1 h to promote the self-assembly of MnO_4^- and CTA^+ on the CNT surface. Finally, 60 mL of ethanol (99%) as reducing agent was added to the precursor solution and maintained at 25 °C for 8 h under stirring. The product was then filtered and washed several times with distilled H_2O, and dried at 100 °C for 10 h. The dried powder was added to a solution of NH_4NO_3 in ethanol at 70 °C for 10 min to remove the CTAB by ion exchange. For comparison, mesoporous MnO_2 oxide was similarly synthesized; 60 mL of ethanol was added to 150 mL of 0.01 M aq. $KMnO_4$ with 1 wt% CTAB and maintained at 25 °C for 8 h under stirring. During the synthesis, the temperature of the solution was maintained at 25 °C with a circulator. The reduction potential of the solution was monitored in situ by measuring the electrode potential (E) with a Pt electrode and a saturated calomel electrode (SCE) using a potentiostat/galvanostat (VMP2, Princeton Applied Research, USA). UV-vis spectroscopy (UV-2401PC, Shimadzu) was used to measure changes in the concentration of MnO_4^- during the synthesis process.

Characterization

Sample structures were determined by X-ray diffraction (XRD) using a diffractometer equipped with a vertical goniometer (D/MAX-IIIC, Rigaku). Scattering angles (2θ) were scanned from 10° to 80° at an interval of 1°. Scanning electron microscopy (SEM, Sirion, FEI) and transmission electron microscopy (TEM, JEM-3000F, JEOL) were used to observe the morphology of the samples. N_2 adsorption–desorption isotherms were measured on a Micromeritics ASAP ZOZO instrument at 77 K, and surface areas were calculated by the Brunauer–Emmett–Teller (BET) method.

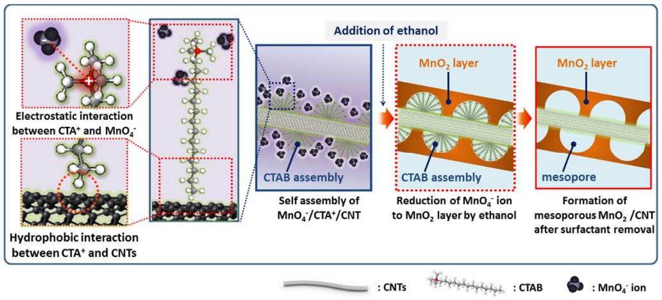

Scheme 1 Schematic illustration of the process used for the synthesis of the meso-MnO_2/CNT composite.

The electrochemical properties at room temperature were investigated using a three-electrode cell with a Pt plate as the counter electrode and an SCE as the reference electrode. The working electrode was prepared by slurry casting onto Ti foil with 90 wt% active material (mesoporous MnO_2/CNT, or mesoporous MnO_2) and 10 wt% polyvinylidene fluoride (PVDF) dissolved in *N*-methyl-2-pyrrolidone (NMP) as a binder. No conductive additives such as carbon black were added to the electrode. The mass of the electrode materials coated onto the Ti foil was approximately 1 mg cm^{-2}. Cyclic voltammetry (CV) and electrochemical impedance spectroscopy (EIS) were conducted in an aqueous 2 M Na_2SO_4 electrolyte solution using a potentiostat/galvanostat (VMP3, Princeton Applied Research) at potential scan rates ranging from 10 to 1,000 mV s^{-1} in a potential window of 0.0–0.9 V vs. SCE. The specific capacitance was calculated from the voltammetric charge of the CV curves. EIS measurements were carried out in the frequency range of 100 kHz to 100 mHz at 0 V vs. SCE with an ac perturbation of 5 mV. The values were normalized based on the weight of active material rather than the area of the electrode.

Results and discussion

The synthetic mechanism for the mesoporous MnO_2/CNT composite (denoted as meso-MnO_2/CNT) is shown in Scheme 1. First, bare CNTs were dispersed with the aid of CTAB; the reagent dissociates to CTA^+ and Br^- ions in aqueous solution, with the CTA^+ species orienting so that the hydrophobic tail group faces toward the CNT surface, while the hydrophilic head group faces outward toward the aqueous phase. The surfactant therefore introduces electrostatic and/or steric repulsion between the individual CNTs, overcoming the van der Waals attractions. In addition, positively charged CTA^+ and negatively charged MnO_4^- ions can self-assemble on the CNT surface. Evidence for the formation of the MnO_4^-/CTA^+/CNT can be found in the SEM and TEM images, and the FT-IR and UV-vis spectra in the supplementary information (Fig. S1, ESI†). After complete reduction of MnO_4^- ions to MnO_2 by ethanol,[19] residual surfactant was removed by ion exchange in ethanolic NH_4NO_3, leaving open mesopores.

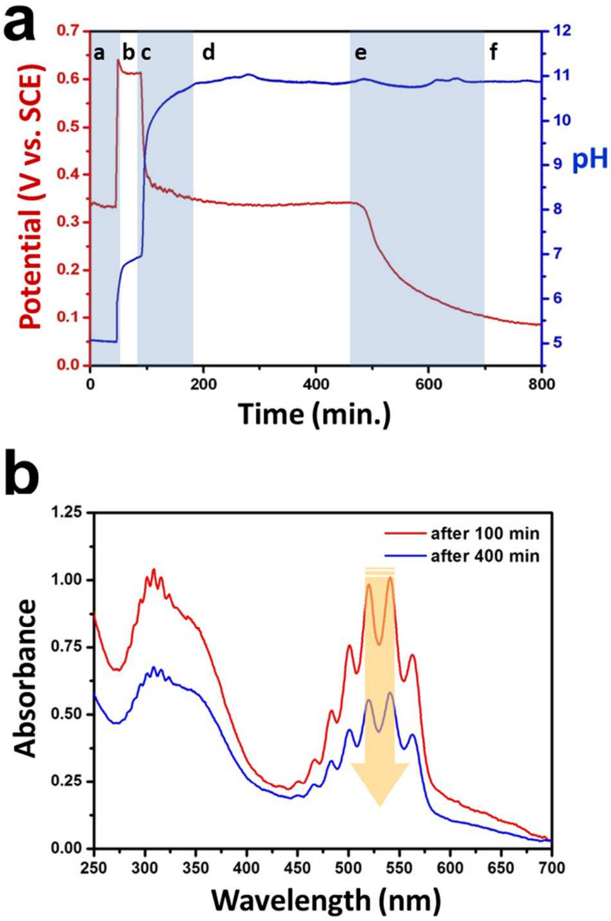

Fig. 1 (a) Electrode potential (E) and pH vs. time curves for meso-MnO_2/CNT measured during the reduction of MnO_4^- ions, (b) UV-vis spectra of the solution sampled at 100 and 400 min.

In this study, ethanol is used as a reducing agent for converting MnO_4^- ions to MnO_2; the proposed reduction mechanism for this approach is as follows:

$$4MnO_4^- + 3C_2H_5OH \rightarrow 4MnO_2 + 3CH_3COOH + 4OH^- + H_2O$$

In order to verify the synthesis mechanism, in situ monitoring of the reduction potential (E) and solution pH was conducted. Fig. 1a shows the changes in electrode potential (E) and solution pH with time during the synthesis of meso-MnO_2/CNT; the figure is divided into six regions (a–f), taking both parameters into consideration. When the $KMnO_4$ solution was added to the aqueous CTA^+/CNT suspension, a rapid increase in both E and pH were observed in region (a). This observation is attributed to basic sites on the CNT surface consisting of delocalized π electrons, which are responsible for the rise in pH in this region as they can act as Lewis bases capable of proton complexation. In region (b), during formation of the MnO_4^-/CTA^+/CNT complex, the plateau region of the E curve corresponds to the reduction potential of MnO_4^- ions in solution is observed.[14]

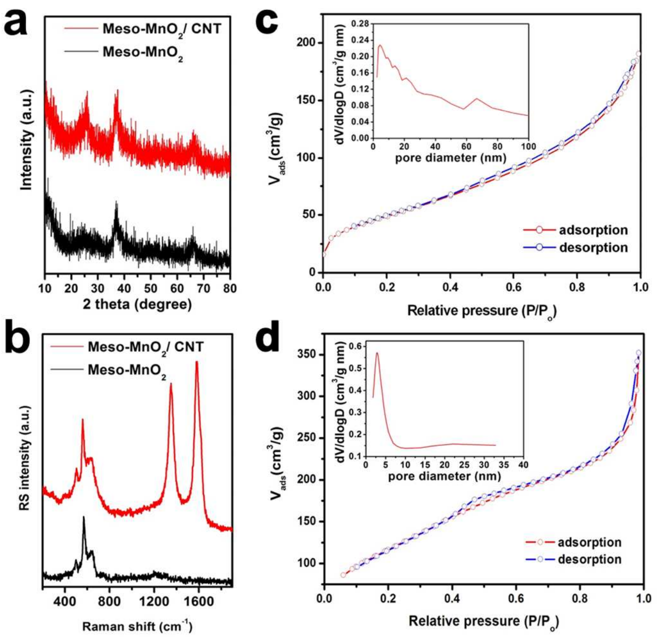

Fig. 2 (a) XRD patterns, (b) Raman spectra of meso-MnO_2/CNT and meso-MnO_2 and N_2 adsorption–desorption isotherms of (c) the meso-MnO_2/CNT composite, and (d) meso-MnO_2.

In region (b), it should be noted that electrode potential (E) and pH stayed constant, which indicates that the CTAB could protect the CNTs from MnO_4^- ions and effectively prevent redox reaction between CNT and MnO_4^- ions. In region (c), ethanol was added to the MnO_4^-/CTA^+/CNT solution and a rapid drop in E was observed, with a concurrent increase in pH owing to the generation of OH^- ions during the reduction of MnO_4^- to MnO_2. The pH then remained relatively constant throughout regions (d–f). As for the reduction rate, it slows down with time and it becomes very low in region (d). In region (d), OH^- ions are generated but relatively slowly compared to those in region (c). Since pH value is based on a logarithmic scale, the pH of solution in region (d) should increase with time, however, the increase is expected to be very small. Therefore, the slight change in pH during the reduction could be explained. Region (d) exhibited a potential plateau with respect to time, which represents the reduction of MnO_4^- ions to MnO_2 by ethanol, and has a value corresponding to the standard reduction potential of MnO_4^- ions under basic conditions.[20]

To monitor the change in solution MnO_4^- concentration during the synthesis process, UV-vis spectroscopy was carried out at different time points. Fig. 1b shows the UV-vis spectra after the addition of ethanol to the MnO_4^-/CTA^+/CNT solution; small amounts of the solution were sampled at 100 and 400 min and cooled rapidly to 4 °C to prevent any further reaction. The absorption spectra were then measured to quantify the MnO_4^- ions remaining. The absorption bands at wavelengths of 525, 545, and 570 nm in Fig. 1b are characteristic of MnO_4^-, and their intensity can be seen to decrease gradually with reaction time, indicating a reduction in the concentration of these ions.

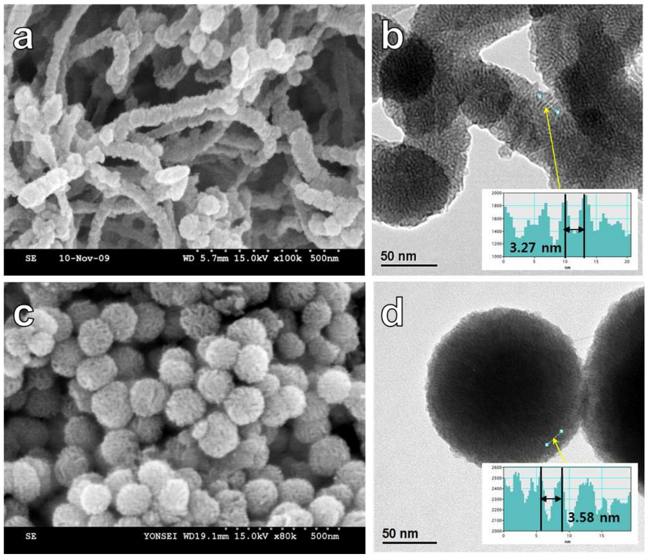

Fig. 3 SEM and TEM images of (a,b) meso-MnO_2/CNT, and (c,d) meso-MnO_2.

A sharp decrease in *E* was seen at the start of region (e), which is indicative of complete reduction of MnO_4^- ions. In region (f), a slight decrease in *E* was observed, reaching a value that corresponds to the equilibrium in aqueous solution after the reaction for given electrochemical cells. After this point, there was no further reaction. For comparison purposes, mesoporous MnO_2 (denoted as meso-MnO_2) was synthesized using a similar synthetic method. The changes in *E* and pH were found to be very similar to those seen in regions (c–f) of the meso-MnO_2/CNT (Fig. S2b, ESI†).

Fig. 2a shows XRD patterns of the meso-MnO_2/CNT and meso-MnO_2 materials. All samples gave a poorly resolved diffraction pattern, with broad peaks at scattering angles around 37° and 66° (26° for CNTs), indicating that the MnO_2 synthesized at room temperature had a low level of crystallinity due to the absence of long-range order, as is typical for the MnO_6 octahedral framework. In the acquired Raman spectra, three major features due to MnO_2 were observed at 510, 575, and 646 cm^{-1}.[21] m m cannot be used to accurately determine the structure of a material; however, analysis of the Raman spectra in Fig. 2b indicates that all of the MnO_2 thin films prepared in this study exhibited similarities to a birnessite-type MnO_2.[21] The Raman spectrum of meso-MnO_2/CNT showed a D-band at ~1,340 cm^{-1} and a G-band at ~1,610 cm^{-1}, which correspond to the stretching modes of sp^2 and sp^3 hybridized carbon, respectively.[22]

N_2 adsorption–desorption isotherms of the meso-MnO_2/CNT and meso-MnO_2 are shown in Fig. 2c–d. A gas adsorption measurement is the most direct technique to characterize mesoporous materials in terms of specific surface area, pore size distribution, and pore volume, especially in disordered mesoporous materials which could not be determined by low-angle XRD or TEM images. Both meso-MnO_2/CNT and meso-MnO_2 show typical type IV isotherms with well-defined steps between the relative pressure (P/P_0) of 0.4 and 0.8, indicating the existence of mesopores. The BET surface areas were found to be 183 and 429 $m^2\ g^{-1}$, with an average pore size of 3–4 nm. The MnO_2 loading was calculated to be 43 wt% (calculated from the molar feeding ratio of $KMnO_4$ to CNT). For verifying this, the thermogravimetric analysis was carried out for the estimation of MnO_2 loading amount (Fig. S3, ESI†). Considering the loading amount of meso-MnO_2 in the composite, surface areas of meso-MnO_2 and CNTs, the decreased BET surface area could be easily calculated by lever role; the proposed equation is as follows:

$$S_{\text{meso-MnO2/CNT}} = S_{\text{CNTs}}\ \mathbf{x}\ f_{\text{CNTs}} + S_{\text{meso-MnO2}}\ \mathbf{x}\ f_{\text{meso-MnO2}} \quad (1)$$

(S: specific surface area, f: weight fraction)

According to the eq. (1), the calculated specific surface area of meso-MnO_2/CNT is 294 $m^2\ g^{-1}$ (188 $m^2\ g^{-1}$ x 0.58 + 429 $m^2\ g^{-1}$ x 0.43), while the measured specific surface area is of 183 $m^2\ g^{-1}$. However, the weight fraction of CNTs (f_{CNTs}) should be considered as zero in eq. (1), where all the surface of CNTs is fully coated with meso-MnO_2. Therefore, the specific surface area of meso-MnO_2/CNT should be calculated to be 184 $m^2\ g^{-1}$ (188 $m^2\ g^{-1}$ x 0 + 429 $m^2\ g^{-1}$ x 0.43) and this calculated value shows good agreement with measured one.

Compared with CNTs or non-porous MnO_2/CNT, the meso-MnO_2/CNT shows the totally different N_2 adsorption–desorption isotherms. While CNTs and non-porous MnO_2/CNT also show the type IV isotherms, significant differences are observed among the CNTs, non-porous MnO_2/CNT and meso-MnO_2/CNT. The CNTs show a hysteresis mainly at relative pressure of 0.8-1.0, which indicates the existence of macropores due to entangled CNTs with most pores in the range of 40-60 nm and little fraction of mesopores around 10 nm. It should be noted that the non-porous MnO_2/CNT shows the similar adsorption–desorption isotherms and pore-size distributions to the CNTs. The CNTs and non-porous MnO_2/CNT have the BET surface areas of 188 and 101 $m^2\ g^{-1}$, respectively (Fig. S4a-b, ESI†). The non-porous MnO_2/CNT with 46 wt.% of loading amount was synthesized following procedures available in the literature.[14, 15]

For the further characterization of mesoporosity of meso-MnO_2/CNT, low-angle XRD were measured (Fig. S4c, ESI†). Comparison of the low-angle XRD patterns of meso-MnO_2/CNT and pristine CNT reveals that there exist two small diffraction peaks at 3.4 and 6.8° only for the meso-MnO_2/CNT and no such peaks for the pristine CNT. Therefore, we believe that the two small diffraction peaks at 3.4 and 6.8° observed for the meso-MnO_2/CNT are due to the mesoporous oxide in the meso-MnO_2/CNT. The low-angle XRD patterns of the meso-MnO_2/CNT are similar to those of the lamellar mesoporous structure with 00l reflections as shown in Fig. R1c.[22-24]

The SEM image in Fig. 3a shows that mesoporous MnO_2 was coated uniformly on the CNTs, while the 3D entangled porous structure of the CNTs was preserved. This indicates that the CTA^+ ions effectively assembled with the MnO_4^- ions on the CNT surface, thereby inducing the selective reduction of the mesoporous MnO_2 layer uniformly on the external surface of

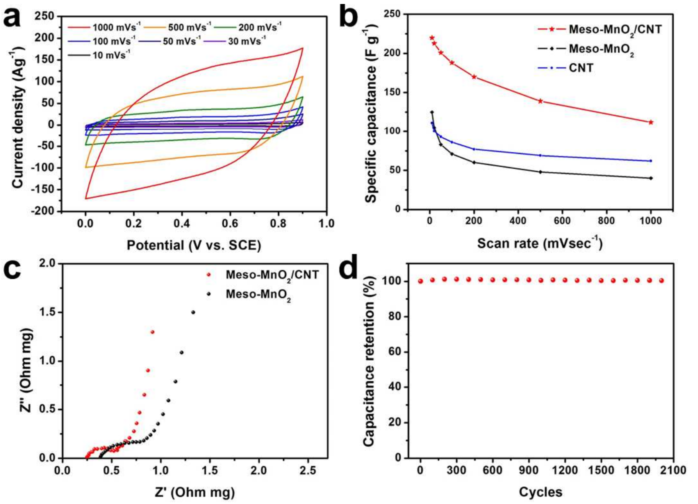

Fig. 4 (a) Cyclic voltammograms of meso-MnO_2/CNT at various scan rates, (b) high rate capability, (c) Nyquist plots of meso-MnO_2/CNT and meso-MnO_2, and (d) cyclability of meso-MnO_2/CNT at 20 A g^{-1}.

the CNTs. The average diameter of the MnO_2-coated CNTs was measured to be ~60 nm. The formation of the mesoporous structure was confirmed using TEM. Fig. 3b shows a typical TEM image of the as-prepared meso-MnO_2/CNT. The diameter of the meso-MnO_2/CNT was measured to be ~60 nm, which is in good agreement with the SEM results. Fig. 3c shows a typical SEM image of meso-MnO_2, which demonstrates that the synthesized material had a uniform spherical shape with a diameter of ~100 nm in the absence of CNTs. Both the as-prepared meso-MnO_2/CNT and meso-MnO_2 shows 3–4 nm of interlayer spacing. After surfactant removal, the meso-MnO_2/CNT and meso-MnO_2 displayed a disordered mesoporous structure, which was caused by partial collapse of the mesoporous domains (Fig. S5, ESI†); however, the overall mesoporous nature was retained.

CV and EIS measurements were used to investigate the electrochemical properties of the meso-MnO_2/CNT and meso-MnO_2 materials. Fig. 4a exhibits CV curves at scan rates ranging from 10 to 1,000 mV s^{-1} in 2.0 M Na_2SO_4. It can be observed that the curves at all of the different scan rates exhibited a typical rectangular shape, indicating ideal capacitive behavior. This shape was even maintained when a scan rate of 1,000 mV s^{-1} was used, with no significant distortion observed, demonstrating a highly reversible system with excellent rate capability.

Fig. 4b shows the specific capacitance values for meso-MnO_2/CNT, meso-MnO_2 and CNTs at different scan rates, calculated from the CV curves. The specific capacitance of meso-MnO_2/CNT at 10 mV s^{-1} was 220 F g^{-1}, and maintained a value of 112 F g^{-1} (approximately 51% of its initial specific capacitance) even at 1,000 mV s^{-1}, indicating an excellent rate capability (Table S1, ESI†). In contrast, the specific capacitance of meso-MnO_2 and CNTs were decreased 125 to 40 F g^{-1} (32% of initial capacitance) and 111 to 62 F g^{-1} (56% of initial capacitance) at 10 and 1,000 mV s^{-1}, respectively. While the meso-MnO_2 shows slightly higher specific capacitance than CNTs, CNTs show better rate capability. Furthermore, calculations based on the amount of MnO_2-active material gave a specific capacitance for the meso-MnO_2/CNT of 512 F g^{-1}, almost five times higher than that for the meso-MnO_2. The meso-MnO_2/CNT has 43 wt.% MnO_2 in the composite and its BET surface area was 183 m^2 g^{-1}. Examination of the SEM and TEM images of the meso-MnO_2/CNT composite indicates that the entire external surface of the CNTs was completely covered with the mesoporous MnO_2. Therefore, it can be assumed that the CNT in the meso-MnO_2/CNT composite did not contribute to the BET surface area. Under this consideration of the loading amount (43 wt.%) of meso-MnO_2 in the composite, the surface area of the meso-MnO_2 in the composite was calculated to be 436 m^2 g^{-1}, while the BET surface area of 429 m^2 g^{-1} for the meso-MnO_2 prepared without the CNTs. Even with the similar specific surface area, the meso-MnO_2/CNT had a specific capacitance of 512 F g^{-1} based on the weight of MnO_2 in the composite, however, the meso-MnO_2 prepared without CNT had a specific capacitance of 112 F g^{-1}. Such a big difference in the specific capacitance between the two different mesoporous oxides is mainly due to the different electrochemical utilization of the electroactive oxides, which is highly dependent on the electrical conductivity of electrodes fabricated using the meso-MnO_2/CNT and the meso-MnO_2 prepared without CNT. Since the meso-MnO_2/CNT was formed to have an intimate and direct contact between the meso-MnO_2 and CNTs during the synthesis, its electrical conductivity is expected to be higher than that of the meso-MnO_2 prepared without CNT. Furthermore, the meso-MnO_2/CNT showed entangled structure of CNTs, which allows electrolyte ions to have ready access to reaction sites. We believe that high electrical conductivity and easy access of ions to reaction sites of the meso-MnO_2/CNT are two other important characteristics that made possible for the meso-MnO_2/CNT to exhibit the far better pseudocapacitive properties compared to meso-MnO_2 prepared without CNT. It has been reported that the incorporation of metal oxides into an electrically conductive carbon framework could improve the electrochemical utilization of oxides.[7, 12, 25-28]

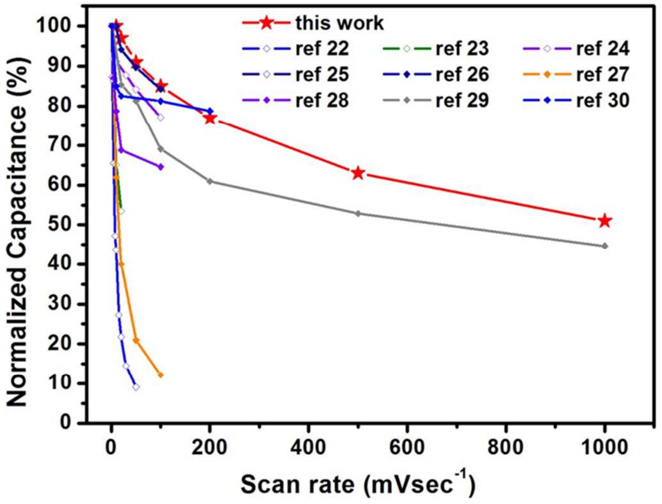

Fig. 5 Comparison of the high rate capabilities of the meso-MnO_2/CNT composite prepared in this study with those of previously reported mesoporous MnO_2 and MnO_2/carbon composite.[27-35]

EIS is a useful technique for analyzing both resistive and capacitive properties. Fig. 4c shows Nyquist plots for the meso-MnO_2/CNT and meso-MnO_2 materials, where it can be seen that the series resistance of the meso-MnO_2/CNT and meso-MnO_2 were 2.54×10^{-3} and 3.77×10^{-3} Ω g, respectively. Assuming that solution resistance and contact resistance are equal, this result means that CNTs can act as an effective current path for improved electrical conductivity of the composite. In addition, the meso-MnO_2/CNT showed lower Z″ values along the vertical section, indicating a higher capacitance than that of meso-MnO_2.[36] Good cycling performance is another crucial factor for energy storage systems. At 20 A g^{-1}, the meso-MnO_2/CNT exhibited excellent cycling performance, with almost no degradation evident after 2,000 cycles (Fig. 4d). This superior cyclability is probably related to the stable mesoporous structure, as the pores can act as a buffer for any volume change that occurs during the process.

Fig. 5 shows the normalized specific capacitance values for meso-MnO_2/CNT and previously reported MnO_2 mateirlas (MnO_2/carbon and mesoporous MnO_2) at different scan rates. Generally, MnO_2/carbon composite shows better rate capability than mesoporous MnO_2. However, the rate capability of MnO_2/carbon composite materials could be further increased when mesoporous structure was introduced. The excellent rate performance of meso-MnO_2/CNT benefits from its improved electrical conductivity as well as the unique mesoporous structure.

Conclusion

In summary, mesoporous MnO_2/CNT composites were successfully synthesized by the reduction of $KMnO_4$ with alcohol using a soft template method. Mesoporous MnO_2 was coated uniformly on the CNTs, providing a high surface area. The electrochemical performance was greatly improved by the synergetic effect of the mesoporous structure and CNTs. The mesopores derived from the MnO_2 and entangled CNT web provided a greater interfacial area between the oxide and electrolyte, improved electron conduction through the CNT web, and allowed for facile ionic transfer within the mesopores. In addition, the 1D interconnected and long-range continuous carbon framework improved the electrical conductivity of the composite, resulting in excellent rate capability and superior cycling stability.

Acknowledgements

This work was supported by the Energy, Efficiency and Resources of the Korea Institute of Energy Technology Evaluation and Planning (KETEP) grant funded by the Ministry of Knowledge Economy, Korean government (No: 20122010100140).

Notes and references

[a] Department of Materials Science and Engineering, Yonsei University 134 Shinchon-dong, Seodaemoon-gu, Seoul 120-749, Republic of Korea. Fax:+82-2-312-5375; Tel: +82-2-365-7745

[b] Energy Efficient Materials Team, Energy & Environmental Division, Korea Institute of Ceramic Engineering & Technology, 233-5 Gasan-dong,
Guemcheon-gu, Seoul 153-801, Republic of Korea. Fax: +82-2-3282-2475; Tel: +82-2-3282-2463; E-mail: rkc@kicet.re.kr

† Footnotes should appear here. These might include comments relevant to but not central to the matter under discussion, limited experimental and spectral data, and crystallographic data.

Electronic Supplementary Information (ESI) available: [details of any supplementary information available should be included here]. See DOI: 10.1039/b000000x/

1. C. T. Kresge, M. E. Leonowicz, W. J. Roth, J. C. Vartuli and J. S. Beck, *Nature*, 1992, **359**, 710-712.
2. D. Zhao, J. Feng, Q. Huo, N. Melosh, G. H. Fredrickson, B. F. Chmelka and G. D. Stucky, *Science*, 1998, **279**, 548-552.
3. D. Zhao, Q. Huo, J. Feng, B. F. Chmelka and G. D. Stucky, *Journal of the American Chemical Society*, 1998, **120**, 6024-6036.
4. Z. R. Tian, W. Tong, J. Y. Wang, N. G. Duan, V. V. Krishnan and S. L. Suib, *Science*, 1997, **276**, 926-930.
5. P. D. Yang, D. Y. Zhao, D. I. Margolese, B. F. Chmelka and G. D. Stucky, *Nature*, 1998, **396**, 152-155.
6. J. Y. Luo, J. J. Zhang and Y. Y. Xia, *Chemistry of Materials*, 2006, **18**, 5618-5623.
7. S.-B. Ma, K.-W. Nam, W.-S. Yoon, X.-Q. Yang, K.-Y. Ahn, K.-H. Oh and K.-B. Kim, *Journal of Power Sources*, 2008, **178**, 483-489.
8. K. W. Nam, C. W. Lee, X. Q. Yang, B. W. Cho, W. S. Yoon and K. B. Kim, *Journal of Power Sources*, 2009, **188**, 323-331.
9. K. Ding, B. Hu, Y. Xie, G. An, R. Tao, H. Zhang and Z. Liu, *Journal of Materials Chemistry*, 2009, **19**, 3725.
10. Z. Y. Sun, H. Y. Zhang, Y. F. Zhao, C. L. Huang, R. T. Tao, Z. M. Liu and Z. D. Wu, *Langmuir*, 2011, **27**, 6244-6251.
11. M. Zhang, Y. Wu, X. Feng, X. He, L. Chen and Y. Zhang, *Journal of Materials Chemistry*, 2010, **20**, 5835.
12. S. M. Bak, K. H. Kim, C. W. Lee and K. B. Kim, *Journal of Materials Chemistry*, 2011, **21**, 1984-1990.

13. S. Ko, J. I. Lee, H. S. Yang, S. Park and U. Jeong, *Advanced materials*, 2012, **24**, 4451-4456.
14. S.-B. Ma, K.-Y. Ahn, E.-S. Lee, K.-H. Oh and K.-B. Kim, *Carbon*, 2007, **45**, 375-382.
15. S.-B. Ma, Y.-H. Lee, K.-Y. Ahn, C.-M. Kim, K.-H. Oh and K.-B. Kim, *Journal of The Electrochemical Society*, 2006, **153**, C27-C32.
16. X. K. Huang, H. J. Yue, A. Attia and Y. Yang, *Journal of the Electrochemical Society*, 2007, **154**, A26-A33.
17. X. Jin, W. Zhou, S. Zhang and G. Z. Chen, *Small*, 2007, **3**, 1513-1517.
18. J. Yan, Z. J. Fan, T. Wei, W. Z. Qian, M. L. Zhang and F. Wei, *Carbon*, 2010, **48**, 3825-3833.
19. V. Subramanian, H. W. Zhu and B. Q. Wei, *Chem Phys Lett*, 2008, **453**, 242-249.
20. J.-M. Lin, F. Qu and M. Yamada, *Anal Bioanal Chem*, 2002, **374**, 1159-1164.
21. C. Julien, M. Massot, R. Baddour-Hadjean, S. Franger, S. Bach and J. P. Pereira-Ramos, *Solid State Ionics*, 2003, **159**, 345-356.
22. C. W. Lee, K. W. Nam, B. W. Cho and K. B. Kim, *Microporous and Mesoporous Materials*, 2010, **130**, 208-214.
23. K. S. Choi, H. C. Lichtenegger, G. D. Stucky and E. W. McFarland, *Journal of the American Chemical Society*, 2002, **124**, 12402-12403.
24. Y. W. Tan, S. Srinivasan and K. S. Choi, *Journal of the American Chemical Society*, 2005, **127**, 3596-3604.
25. S.-B. Ma, K.-W. Nam, W.-S. Yoon, S.-M. Bak, X.-Q. Yang, B.-W. Cho and K.-B. Kim, *Electrochemistry Communications*, 2009, **11**, 1575-1578.
26. R. R. Bi, Y. X. Yin, Y. G. Guo and L. J. Wan, *Journal of Nanoscience and Nanotechnology*, 2011, **11**, 1996-2002.
27. S. W. Lee, J. Kim, S. Chen, P. T. Hammond and Y. Shao-Horn, *Acs Nano*, 2010, **4**, 3889-3896.
28. H. Xia, Y. Wang, J. Y. Lin and L. Lu, *Nanoscale Res Lett*, 2012, **7**, 1-10.
29. S. Li, L. Qi, L. Lu and H. Wang, *RSC Advances*, 2012, **2**, 3298-3308.
30. S. Li, L. Qi, L. Lu and H. Wang, *RSC Advances*, 2012, **2**, 6741-6743.
31. Q. Zhou, X. Li, Y.-G. Li, B.-Z. Tian, D.-Y. Zhao and Z.-Y. Jiang, *Chinese Journal of Chemistry*, 2006, **24**, 835-839.
32. C. Yuan, B. Gao, L. Su and X. Zhang, *Journal of Colloid and Interface Science*, 2008, **322**, 545-550.
33. Y. Wang, H. Liu, X. Sun and I. Zhitomirsky, *Scripta Materialia*, 2009, **61**, 1079-1082.
34. X. F. Xie and L. Gao, *Carbon*, 2007, **45**, 2365-2373.
35. M. N. Patel, X. Q. Wang, D. A. Slanac, D. A. Ferrer, S. Dai, K. P. Johnston and K. J. Stevenson, *Journal of Materials Chemistry*, 2012, **22**, 3160-3169.
36. J. H. Chae and G. Z. Chen, *Particuology*.